Conformational Dynamics and Thermal Cones of C-terminal Tubulin Tails in Neuronal Microtubules

Danko D. Georgiev[1] and James F. Glazebrook[2]

November 7, 2007

[1] Laboratory of Molecular Pharmacology, Faculty of Pharmaceutical Sciences, Kanazawa University Graduate School of Natural Science and Technology, Kakuma-machi, Kanazawa, Ishikawa 920-1192, JAPAN
E-mail: danko@p.kanazawa-u.ac.jp

[2] Department of Mathematics and Computer Science, Eastern Illinois University, 600 Lincoln Avenue, Charleston, Illinois 61920-3099, USA
E-mail: jfglazebrook@eiu.edu

Abstract

In this paper we present a model for estimation of the C-terminal tubulin tail (CTT) dynamics in cytoskeletal microtubules of nerve cells. We show that the screened Coulomb interaction between a target CTT and the negatively charged microtubule surface as well as its immediate CTT neighbours results in confinement of the CTT motion within a restricted volume referred to as a thermal cone. Within the thermal cone the CTT motion is driven by the thermal fluctuations, while outside the thermal cone the CTT interaction energy with its environment is above the thermal energy solely due to repulsion from the negatively charged microtubule surface. Computations were performed for different CTT geometries and we have found that the CTT conformation with lowest energy is perpendicular to the microtubule surface. Since the coupling between a target CTT with its neighbour CTTs is 8 orders of magnitude below the thermal energy and considering the extremely short cytosolic Debye length of 0.79 nm, our results rule out generation and propagation of CTT conformational waves along the protofilament as a result of local CTT perturbations. The results as presented support a model in which the cytosolic electric fields and ionic currents generated by the neuronal excitations are "projected" onto the CTTs of underlying microtubules thus affecting their regulatory function upon kinesin motion and MAP attachment/detachment.

Originally published in *Neuroquantology* 2007; **5**(1): 62-84.

1 Introduction

Current wisdom in neuroscience holds that the electric excitations of nerve cells affect directly the function only of a certain class of membrane proteins known as voltage gated ion channels. The huge electric field between the inner and outer phospholipid layers of the plasma membrane was shown to regulate the opening and closure of those channels (Hille, 2001). Only recently emerged novel possibilities such as direct regulation of the function of some cytoskeletal proteins by the neuronal cytosolic currents and electromagnetic field by affecting the conformational status of portions of the tubulin molecule that have a form of enzymatic activity (Georgiev and Glazebrook, 2006).

The neuronal cytoskeleton is the major internal structure that defines the external shape and polarity of the nerve cell and organizes its cytoplasm to perform motile and metabolic activities essential to life. The constituents of the cytoskeleton consist of microtubules, intermediary filaments, actin, microtubule-associated proteins (MAPs), motor proteins, cross-linking proteins (e.g. the plakin superfamily), various cytoskeletal scaffold proteins and cytoskeletal-bound enzymes (Vale et al., 1992). Microtubules form the major component of the cytoskeleton and are composed from tubulin, a heterodimer of two subunits, types α and β (Nogales, 2000). Microtubules organize the cellular shape which is vital for neurons in stabilizing their cable-like projections called neurites (dendrites or axons). They also provide anchors for compartmentalization of various enzymes including some of those involved in glycolysis (Lloyd and Hardin, 1999), different phosphatases or kinases, etc. (Sontag et al., 1999), and serve as tracks and regulators of the function of motor proteins (such as kinesin, dynein, etc.) which drive cargo vesicles that transport various proteins and structural components of the plasma membrane or the extracellular matrix of neurons (Hirokawa, 1998).

Part of the vital functions performed by microtubules can be attributed to the tiny C-terminal tubulin tails (CTTs) projecting from each tubulin monomer. Experiments have shown that CTTs are effective catalysts controlling the kinesin walk (Skiniotis et al., 2004). Subtilisin treated microtubules that lack CTTs bind stably and can be decorated by ADP-kinesin molecules, while normal microtubules do not bind ADP-kinesin (ADP abbreviates adenosine diphosphate). This suggests that CTTs catalyze the ADP-kinesin detachment from the microtubule surface accounting for the kinesin motion along the protofilament. Similarly CTTs could catalyze detachment of phosphorylated MAP molecules from the microtubule surface. Based on recently proposed classification of enzymes (Purich, 2001) one might consider CTTs as *energases* - enzymes that make or break noncovalent bonds in the interaction partner (often being protein complex composed of several subunits), therefore triggering conformational transition that affects directly the function of the partner. Noncovalent are the hydrogen bonds and the weak van der Waals forces, therefore in the action of energases of great importance should be the quantum tunneling effects between different conformations.

CTTs and microtubule-associated protein 2 (MAP-2) belong to a group of

proteins that are considered to be "natively disordered" however their biological function may depend on the potential for flipping from disordered into an ordered coil state (Uversky, 2002). In this situation the biology waits for physical modeling and the creation of theoretical toy models is of great importance since the direct *in vitro* nuclear magnetic resonance (NMR) exploration of the protein usually reveals no order that indeed could be manifested *in vivo*. Considering the need for biophysical modeling we have undertaken a theoretical study of the possible collective behavior of the CTTs in the cytoskeletal microtubules and we searched for possible generation and sustained propagation conformational waves along the outer microtubule surface. In previous publications we have reported a novel model in which the intraneuronal electric activity was described in terms of traveling electromagnetic waves (solitons) that were "projected" onto the CTT conformational status (Georgiev et al., 2004; Georgiev and Glazebrook, 2006). It was shown that the bioelectric processes (dendritic and axonal membrane potentials and cytosolic currents) might affect the CTTs of the underlying cytoskeletal microtubules in such a fashion that results in traveling conformational wave along the CTTs. In this paper we try to answer the question whether it is possible for a local electrostatic factor (e.g. the interaction between a CTT and a charged macromolecule such as MAP-2, kinesin, dynein, etc., or CTT binding to a positively charged microtubule surface spot) to induce propagation of a conformational wave along the microtubule CTTs. If such local perturbations were able to propagate along the CTT protofilament in a certain sense this would corrupt the information inputted to the CTTs by the neuronal electric excitations. The results presented in the following discussion rule out such a possibility and underline the importance of the electric processes in neurons as the only possible mechanism for generation of collective CTT motion.

2 Theory

2.1 Debye-Hückel electrostatic screening in cytosol

In order to address the problem, we should take into consideration the actual *in vivo* conditions of the neuronal interior (cytosol). The cytosol has the properties of an electrolyte solution therefore the electrostatic interaction between charged macromolecules will be screened by the formation of dynamic counter-ion shells. The first theoretical treatment of screening due to Debye and Hückel (1923) dealt with a stationary point charge embedded in a fluid. We recall some of the basic principles of the theory. In a fluid composed of electrically charged constituent particles, each two particles interact through the Coulomb force. However, this interaction is suppressed by the flow of the fluid particles in response to electric fields. This flow reduces the effective interaction between the charged particles to a short-range screened Coulomb interaction.

Suppose we have an electrolyte solution at body temperature. At a point x, let $\rho(x)$ denote the charge density of ions, and $\varphi(x)$ denote the electric potential.

The charge density of ions is given by:

$$\rho(x) = q_e \sum_i z_i c_i(x) \tag{1}$$

where $q_e = 1.6 \times 10^{-19} C$ is the elementary charge of proton, z_i is the valency of the ion type i and $c_i(x)$ is the number of ions of type i per unit volume.

At first, the ions are evenly distributed so that there is zero net charge at every point. Therefore $\varphi(x)$ is initially a constant as well. Then we introduce a point charge Q in the electrolyte. The associated charge density is $Q\delta(x)$, where $\delta(x)$ is the Dirac delta function. After the system has returned to equilibrium, let the change in the ion density and electric potential be $\Delta\rho(x)$ and $\Delta\varphi(x)$ respectively. The charge density and electric potential are related by the Poisson equation:

$$-\nabla^2 \left[\Delta\varphi(x)\right] = \frac{1}{\epsilon_0 \epsilon_r} \left[Q\delta(x) + \Delta\rho(x)\right] \tag{2}$$

where $\epsilon_0 = 8.8542 \times 10^{-12} F m^{-1}$ is the dielectric constant of vacuum, and $\epsilon_r = 74.31$ is the relative dielectric constant of water at body temperature.

To proceed, we must find a second independent equation relating $\Delta\rho(x)$ and $\Delta\varphi(x)$. In the Debye-Hückel approximation, we maintain the system in thermodynamic equilibrium, at a temperature T high enough that the fluid particles obey Maxwell-Boltzmann statistics. The number of ions per unit volume $c_i(x)$ depends on the Brownian motion of the ions and is described by the Boltzmann distribution:

$$c_i(x) = c_i^\infty \exp\left(-\frac{z_i q_e \varphi(x)}{k_B T}\right) \tag{3}$$

where $k_B = 1.3807 \times 10^{-23} J K^{-1}$ is the Boltzmann constant, $T = 310K$ is body temperature, c_i^∞ is the number of ions i per unit volume at an infinite distance or at any reference position where the potential of mean force $w_i = z_i q_e \varphi(x)$ is set to zero (Fogolari et al., 1999). For $\rho(x)$ then we have:

$$\rho(x) = q_e \sum_i z_i \left[c_i^\infty \exp\left(-\frac{z_i q_e \varphi(x)}{k_B T}\right)\right] \tag{4}$$

The condition $\frac{w_i}{k_B T} \ll 1$ permits us to truncate after the first term of the power series expansion:

$$\rho(x) = q_e \sum_i z_i c_i^\infty - \frac{q_e^2 \varphi(x)}{k_B T} \sum_i z_i^2 c_i^\infty \tag{5}$$

The first term $q_e \sum_i z_i c_i^\infty$ is zero because of the electrical neutrality of the electrolyte solution[1], so we can simplify to:

[1]This might not be the case under depolarization or hyperpolarization of the neuron, therefore the neuronal electric activity must be critical for the CTT conformations.

$$\rho(x) = -\frac{q_e^2 \varphi(x)}{k_B T} \sum_i z_i^2 c_i^\infty \tag{6}$$

Taking into account the Poisson equation relating $\rho(x)$ and $\varphi(x)$ in the form $\frac{\partial^2 \varphi(x)}{\partial x^2} = -\frac{\rho(x)}{\epsilon_0 \epsilon_r}$, we obtain $\frac{\partial^2 \varphi(x)}{\partial x^2} = \kappa_D^2 \varphi(x)$, where

$$\kappa_D^{-1} \equiv \sqrt{\frac{\epsilon_0 \epsilon_r k_B T}{q_e^2 \sum_i z_i^2 c_i^\infty}} \tag{7}$$

is the Debye length of the electrolyte solution.

Now for the change in the ion density $\Delta\rho(x)$ and the change of the electric potential $\Delta\varphi(x)$ after the introduction of the point charge Q, we have the relation:

$$-\Delta\rho(x) = \epsilon_0 \epsilon_r \kappa_D^2 \Delta\varphi(x) \tag{8}$$

Substitution back in eq. (2) gives us:

$$\left[\nabla^2 - \kappa_D^2\right] \varphi(x) = -\frac{Q\delta(x)}{\epsilon_0 \epsilon_r} \tag{9}$$

The solution is:

$$\varphi(x) = \frac{Q}{4\pi\epsilon_0 \epsilon_r x} \exp\left[-\kappa_D x\right] \tag{10}$$

Thus within the framework of the linear Poisson-Boltzmann theory the interaction energy $U(x)$ between two screened point charges q_1 and q_2 is given by:

$$U(x) = \frac{q_1 q_2}{4\pi\epsilon_0 \epsilon_r x} \exp\left[-\kappa_D x\right] \tag{11}$$

2.2 Debye length of neuronal cytosol

In order to make a feasible estimation for the value of the Debye length of the neuronal cytosol we use the fact that the cytosol osmolarity is 290 mOsm/l. The presence of divalent ions strongly diminishes the value of κ_D^{-1} therefore we have to consider the concentration of the Mg^{2+}, Ca^{2+} and HPO_4^{2-} ions inside the neuronal cytosol. In resting neurons the concentration of free Mg^{2+} ions is 0.5 mM (Brocard et al., 1993), while the free Ca^{2+} concentration is just 0.2 μM (Zeng and Liu, 1993). Neurons use a Na^+-dependent inorganic phosphate cotransporter to import phosphate ions inside the cell, therefore the free cytosolic HPO_4^{2-} ion concentration is greater than the plasma concentration of phosphate ions and its value is above 1 mM. Since the concentration of other divalent ions in cytosol is negligible, we estimate that only 0.5% of the diffusible intracellular ions are divalent. After numerical substitution in eq.(7) we obtain that the Debye length for neuronal cytosol is $\kappa_D^{-1} = 0.79$ nm.

3 Method

3.1 Modeling the screened tail-tail coupling

The precise geometry of the microtubules *in vivo* was established with sufficient accuracy up to several angstroms. The tubulin monomer length inside the microtubule wall is $l_T = 4.05$ nm (Hyman et al., 1995) and the longitudinal displacement between two tubulin monomers in adjacent protofilaments is $\xi_{PF} = 0.92$ nm (Erickson and Stöffler 1996). The space between the centers of two neighbouring tubulin monomers located in neighbouring protofilaments can be calculated if we know the value of the microtubule diameter d_{MT} that is 24 nm for 13 protofilament microtubules (Diaz et al., 1998; de Pablo et al., 2003).

The CTTs are considered to be disordered polypeptides extending out of the microtubule outer surface (Bhattacharyya et al., 1985; Sackett and Wolff, 1986). Their length may vary depending on the environmental conditions between 3-6 nm as estimated according to the presented data on the polypeptide length by Pauling et al. (1951) and considering the effect of nearby counter ions on the length of polyelectrolyte brushes (Chitanvis, 2003; O'Shaughnessy and Yang, 2005). Because of the acidic character of the CTTs at physiological pH=7 they are negatively charged. Since the tubulin outer surface is also negatively charged (Baker et al., 2001) the CTTs are repelled and thus project out in a direction perpendicular to the microtubule surface. A computer generated geometrical model of an assembled 13-protofilament 3 start-helical "haired" microtubule was developed by Georgiev et al. (2004) and presented here as Figure 1.

Each CTT is surrounded by 8 CTT neighbours and experiences the screened electrostatic field generated by those neighbours. In the computation we model each CTT as composed from a non-charged stiff lever backbone and 10 equidistantly spaced negative elementary electric charges q_e contributed by negatively charged COO^- groups.

Each charged COO^- group is not located on the main CTT stalk, instead it resides on the top of an aminoacid side chain. *In vivo* the CTT COO^- groups are contributed either by glutamate (E) or aspartate (D) residue. In order to simplify the computation we have modeled all COO^- groups as being contributed by glutamates, therefore located on non charged aminoacid side chain arm with length of 0.45 nm. This approach is satisfactory since there are only occasionally aspartates in the different CTT isotypes (see Table 1). Preliminary computations that took into account the minor α or β tubulin isotype differences did not reveal a noticeable change in the interaction energies. Furthermore, we will describe a geometric model used for both isotypes of tubulin tails.

Solution studies showed that the helical propensity of β-CTT could be extended for at least 9 more residues (Jimenez et al., 1999) compared to the structure reported in the crystallographic model (Nogales et al., 1998). Thus in the base of the β-CTT there is a nine aminoacid sequence 423-431 (QQYQDATAD) that might undergo coil-to-helix transition, and thus increase or decrease the CTT length. Due to electrostatic repulsion between the β-tubulin body and the glutamate residues located in the β-CTT base the hydrogen bonds stabi-

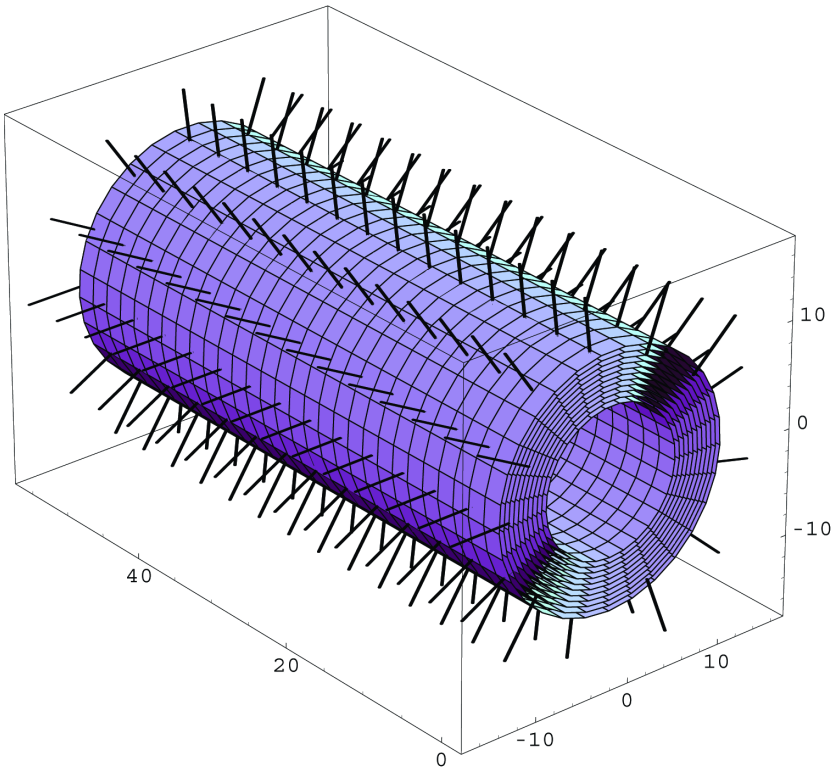

Figure 1: Computer generated model of a 60 nm long segment of 13 protofilament 3-start helical left handed "haired" microtubule. Outer microtubule diameter of 24 nm, inner diameter of 14 nm, microtubule wall thickness of 5 nm, and C-terminal tubulin tail (CTT) length of 5 nm. CTTs extending from each protofilament are visualized as rows of hairy projections.

Table 1: C-terminal aminoacid sequences for different human tubulin isotypes; protein sequences are obtained from PubMed (Gene).

Tubulin isotype	Aminoacid sequence
α_1(431-448)	DYEEVGIDSV EDEDEGEE
α_2(431-450)	DYEEVGVDSV EAEAEEGEEY
α_3(431-451)	DYEEVGVDSV EGEGEEEGEE Y
α_6(431-449)	DYEEVGADSA DGEDEGEEY
α_8(431-449)	DYEEVGTDSF EEENEGEEF
β_1(431-451)	VLEEDEEVTE EAEMEPEDKG H
$\beta_{2a/2b}$(431-445)	DEQGEFEEEE GEDEA
β_{2c}(431-445)	EEEGEFEEEA EEEVA
β_3(431-450)	EEEGEMYEDD EEESEAQGPK
β_4(431-444)	EEGEFEEEAE EEVA
β_5(431-444)	EEEEDFGEEA EEEA
β_6(431-446)	NDGEEAFEDE EEEIDG
β_8(431-444)	EEEEDEEYAE EEVA

lizing the last 3.6 aminoacid turn of the putative nine aminoacid α-helix are expected to break down. Thus the aminoacids 428-431 of the β-CTT should be permanently in extended coil state contributing a flexible noncharged base of approximately 1 nm length for the β-CTT. This helix-to-coil flip is sufficient to minimize the interaction energy between the β-tubulin body and the β-CTT making it comparable to or less than k_BT. Inspection of the base of the α-CTT also shows that the predominant aminoacid residues are not charged ones. Therefore we can use a simplified model for both CTTs in which we consider non-charged CTT base with length of 1 nm with the subsequent 10 glutamate side chains protruding from the main stalk at 0.4 nm spacing (Figure 2). In order to facilitate the analytic treatment of the model the CTT main stalk is considered as a stiff rod with fixed length of 5 nm.

For the subsequent discussion we need a Cartesian coordinate system attached to the microtubule. So we choose a target CTT with base centered at the origin $\mathcal{O}(0,0,0)$. The direction pointing towards the microtubule minus end (capped by α-tubulin subunits) will be denoted as $+x$ direction. The direction perpendicular to and pointing away from the microtubule surface at the point $\mathcal{O}(0,0,0)$ will be denoted as $+z$ direction. The $+y$ direction is defined in such a fashion that the x, y, and z axes form right-handed coordinate system.

The COO^- glutamate groups of each CTT are located on the top of aminoacid side chains. We have considered different types of COO^- ordering each possessing a minimized COO^- repulsion within the tail. This is possible when the COO^- groups have a spiral ordering and the distance between the COO^- groups is greater than the *Bjerrum length* λ_B given by:

$$\lambda_B = \frac{q_e^2}{4\pi\epsilon_0\epsilon_r k_B T} \tag{12}$$

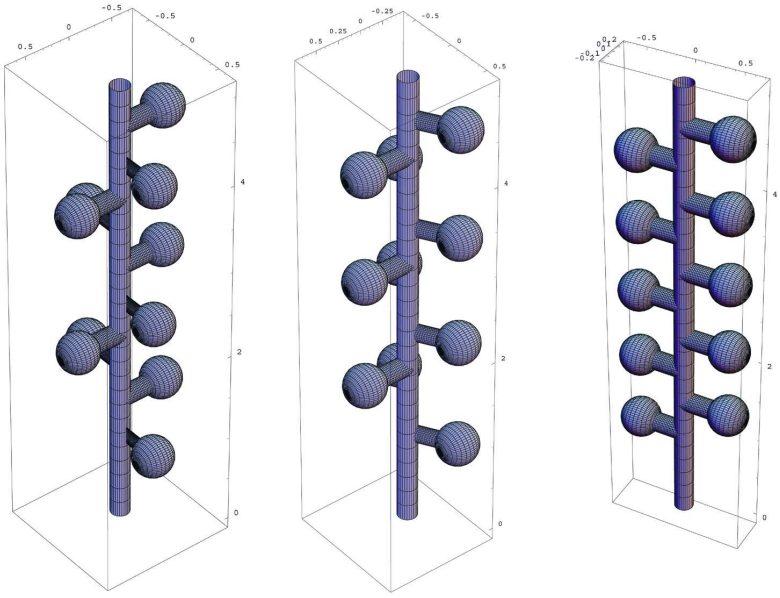

Figure 2: Three different CTT geometries depending on the glutamate COO^- group ordering with corresponding angle ω of the glutamate side chains being $\frac{\pi}{2}$, $\frac{2\pi}{3}$ or π. The CTT length is 5 nm, the glutamate side arms on whose top resides the negatively charged carboxyl group are with length $R = 0.45$ nm. The spiral ordering of the glutamate COO^- groups minimizes the repulsion within the tubulin tail so that each two COO^- groups are separated by distance greater than the Bjerrum length λ_B.

and defined as the distance at which the Coulomb interaction between two non-screened charges equals the thermal energy $k_BT = 4.28 \times 10^{-21}$ J.

We have considered a spiral ordering of the COO^- groups with the lowest COO^- group rotated at angle β_1 from the x-axis when the CTT is perpendicular to the microtubule surface and where each aminoacid side chain arm is rotated by an angle ω relative to its immediate COO^- neighbours. All of the computations were performed for 3 different geometries of the CTTs with corresponding angle ω of the glutamate side chains being $\frac{\pi}{2}$, $\frac{2\pi}{3}$ or π.

The screened Coulomb interaction between a target CTT and its neighbouring CTTs is computed as a sum of the interaction energies between each of the COO^- groups of the target CTT and each COO^- group located on a CTT neighbour. The CTT motion is described by 3 independent parameters: θ is the tilting angle between the z-axis and the CTT main stalk, ϕ is the angle between the x-axis and the orthogonal projection of the CTT main stalk in the xy-plane, and β_1 is angle describing the axial CTT spinning defined as the angle between the lowest COO^- glutamate side arm and the x-axis when the CTT is perpendicular to the xy-plane. It is clear that the interaction energy function of the CTT should be plotted in 4-dimensional space. In order to visualize the CTT interaction energy and the region in which the CTT could be freely driven by the thermal fluctuations, we fix the parameter β_1 and plot the energy surface as a function of the CTT tilting only. With this procedure one can thus visualize an infinite number of 3-dimensional thermal cone plots for different initial angles β_1 belonging to the interval from 0 to 2π.

Since one may have concern about possible noncommutativity of the order of CTT rotations/motions we would like to point out that we describe a model in which the CTT axial spinning is performed in perpendicular position and once the angle β_1 is fixed, the CTT tilts without axial CTT spinning. If we denote the plane defined by the CTT main stalk in perpendicular position to the microtubule surface and the CTT stalk in tilted position as σ-plane, for further clarification we would like to point out that the CTT tilting in the σ-plane without axial rotation around the CTT stalk implies that the angle between the glutamate arm of arbitrary COO^- group and the σ-plane remains invariant during the tilting (i.e. the distance from each COO^- to the σ-plane is invariant). Thus one can recover the position of all COO^- groups knowing the initial position of the lowest COO^- group, the geometry of the spiral ordering described by the angle ω, and the current tilting angles and of the CTT (see Figure 3).

In this model with fixed parameter β_1 the coordinates of an arbitrary group COO_i^- on the target CTT are given by:

$$x_i = R\cos\beta_i + [L_i\cos\theta + R\cos(\phi - \beta_i)(\cos\theta - 1)]\cos\phi \tag{13}$$

$$y_i = R\sin\beta_i + [L_i\cos\theta + R\cos(\phi - \beta_i)(\cos\theta - 1)]\sin\phi \tag{14}$$

$$z_i = L_i\cos\theta - R\cos(\phi - \beta_i)\sin\theta \tag{15}$$

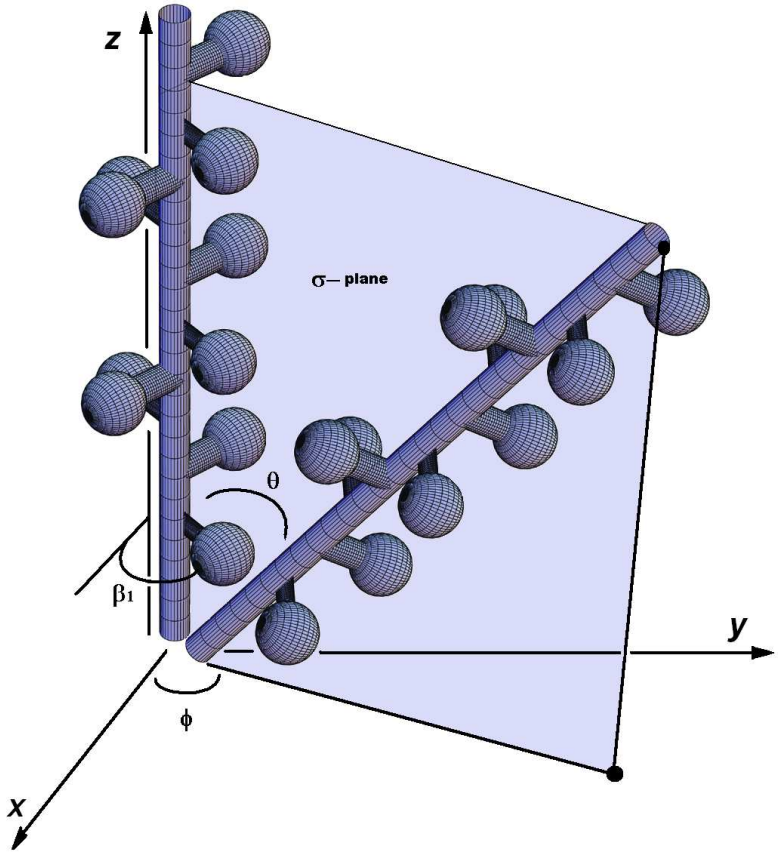

Figure 3: Geometry of the described in the text CTT tilting parameterized by the angles θ, ϕ and β_1.

Table 2: Coordinates of the bases of the CTT neighbours, as well as their tilting angles.

CTT base	x-coordinate	y-coordinate	z-coordinate	θ-angle	ϕ-angle
CTT_1	l_T	0	0	0	0
CTT_2	$l_T - \xi_{PF}$	$-l_Y$	l_Z	$\frac{2\pi}{13}$	$-\frac{\pi}{2}$
CTT_3	$-\xi_{PF}$	$-l_Y$	l_Z	$\frac{2\pi}{13}$	$-\frac{\pi}{2}$
CTT_4	$-l_T - \xi_{PF}$	$-l_Y$	l_Z	$\frac{2\pi}{13}$	$-\frac{\pi}{2}$
CTT_5	$-l_T$	0	0	0	0
CTT_6	$-l_T + \xi_{PF}$	l_Y	l_Z	$\frac{2\pi}{13}$	$\frac{\pi}{2}$
CTT_7	ξ_{PF}	l_Y	l_Z	$\frac{2\pi}{13}$	$\frac{\pi}{2}$
CTT_8	$l_T + \xi_{PF}$	l_Y	l_Z	$\frac{2\pi}{13}$	$\frac{\pi}{2}$

where L_i is the distance between the CTT base and the attachment place of the glutamate side chain of the i$^{\text{th}}$ COO^- group, $R = 0.45$ nm is the length of the glutamate side chain, and $\beta_i = \beta_1 + (i-1)\omega$ is the angle between the i$^{\text{th}}$ COO^- glutamate side arm and the x-axis when the CTT is perpendicular to the xy-plane.

We number the target CTT neighbours in clockwise fashion starting from the CTT neighbour possessing $+x$ coordinate of its base that is located in the same protofilament with the target CTT. The coordinates of the interacting neighbouring COO^- groups are then easily derived if one considers the longitudinal displacement between neighbouring protofilaments ξ_{PF} and the fact that the CTTs in neighbouring protofilaments are perpendicular to the microtubule surface hence tilted by $\frac{2\pi}{13}$ angle from the z-axis. The coordinates of the base and the tilting angles of the CTT neighbours in the model are shown on Table 2, where $l_Y = \frac{d_{MT}}{2} \sin\frac{2\pi}{13}$ and $l_Z = \frac{d_{MT}}{2}\left[\cos\frac{2\pi}{13} - 1\right]$. The computation of the interaction energy plots for different target CTT geometries were performed both for (i) symmetric case with all CTT neighbours being perpendicular to the microtubule surface and modeled with the same initial parameter ω and (ii) asymmetric case in which the CTT neighbours were allowed to have arbitrary chosen (random) set of parameters.

3.2 Modeling the screened CTT-microtubule surface interaction

In order to account for the interaction between the CTT and the microtubule negatively charged outer surface (Baker et al., 2001) we have modeled the microtubule outer surface as a uniformly charged cylindrical surface with charge density σ being 0.5 electron charges per 1 nm^2. Within the framework of the linear Poisson-Boltzmann theory the screened electric potential $\varphi(r)$ at a distance r from the surface of a negatively charged cylinder with surface charge density $\sigma < 0$ is given by:

$$\varphi(r) = -\frac{2k_BT}{q_e b \kappa_D} \frac{K_0\left[\kappa_D\left(\frac{d}{2}+r\right)\right]}{K_1\left[\kappa_D \frac{d}{2}\right]} \tag{16}$$

where d is the diameter of the charged cylinder, b is the *Gouy-Chapman length* given by:

$$b = \frac{q_e}{2\pi|\sigma|\lambda_B} \tag{17}$$

and $K_0(x)$, $K_1(x)$ are *modified Bessel functions* of imaginary argument (see also Hansen and Löwen, 2000; Cherstvy and Winkler, 2004; Poon and Andelman, 2006).

For the interaction energy $U(r)$ between the microtubule surface and an elementary electric charge q_e located at distance r above the microtubule surface we obtain:

$$U(r) = \frac{q_e \sigma}{\kappa_D \epsilon_0 \epsilon_r} \frac{K_0\left[\kappa_D\left(\frac{d}{2}+r\right)\right]}{K_1\left[\kappa_D \frac{d}{2}\right]} \tag{18}$$

With the use of eqs.(11,13-15,18) we have created a computer program for *Wolfram's Mathematica 5.0* that computes the interaction energy plots as a function of the geometry and initial position of the target CTT and the geometry and initial position of the neighbouring CTTs. The interaction energy of each CTT was plotted as a function of the CTT top projection on the xy-plane in a spatial region of 3.5×3.5 nm. The choice to work within the framework of the linear Poisson-Boltzmann theory except that it is easier for analytic treatment is based also on the fact that the percent of divalent ions in the cytosol is very low and more importantly the linear Poisson-Boltzmann theory leads to closely matching predictions with those done by the nonlinear theory for distances h between the interacting charged objects satisfying $\kappa_D h > 1$, which is clearly the case for microtubules and CTTs (for details on the differences between nonlinear Poisson-Boltzmann theory vs. linear one we refer the reader to the excellent paper by Stankovich and Carnie, 1996).

4 Results

4.1 The role of COO^- group geometry in CTT dynamics

In order to estimate the CTT dynamics we have considered a target CTT surrounded by 8 neighbouring CTTs, all of them possessing the same CTT geometry (parameter ω), and all of them being perpendicular to the microtubule surface facing up with their lowest COO^- group in the same direction (parameter β_1). We have computed the interaction energy plots for all the three CTT geometries in which the target CTT and its neighbours were allowed to face up to differing initial directions. Fixing the parameter β_1 of the target CTT allows the interaction energy surface to be computed as a function only of the tilting angles θ

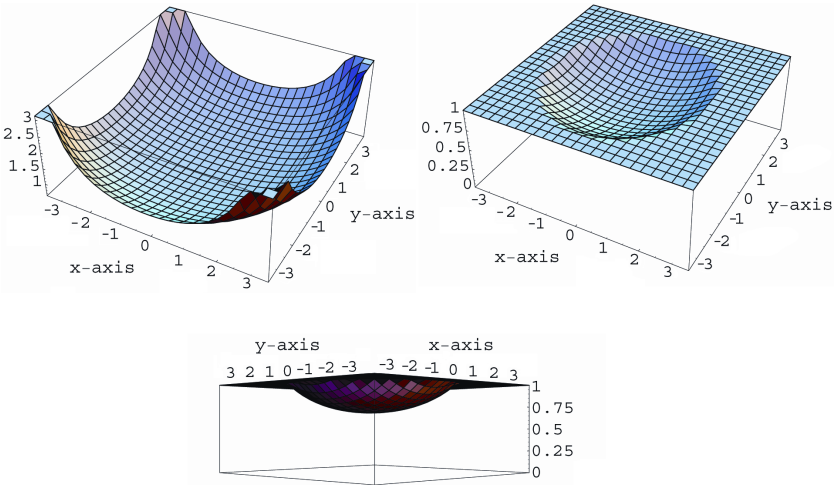

Figure 4: (a) Interaction energy in k_BT units of a target CTT with its environment as a function of the CTT top projection on the xy-plane. (b-c) The thermal cone is visualized by setting the plot range from 0 to 1 k_BT. Depicted is a spatial region with dimensions 3.5×3.5 nm.

and ϕ, and therefore as a function of the x- and the y-coordinate of the top of the target CTT. The computation shows that the minimal interaction energy with the neighbouring CTTs and the microtubule surface has the vertical CTT conformation perpendicular to the microtubule surface. The CTT can explore the space around its origin, and the tilting angle θ must exceed $\frac{\pi}{5}$ radians in order for the interaction energy between the target CTT and its environment to overcome the thermal fluctuations.

The comparison between the three different CTT geometries (as well as the different initial orientations of the target CTT) showed no difference in the resulting interaction energy plots as can be explained by the extremely low coupling between the neighbouring CTTs being 8 orders of magnitude below k_BT. In assymetric trials with randomly chosen parameters for the CTT neighbours under which the CTTs neighbours remain in their thermal cones also revealed no significant change in the interaction energies. The resulting plots of the interaction energy and the thermal cone are identical for all the three CTT geometries in all trials and are presented all together as Figure 4 in order to avoid repetition of identical images.

Further computations of the tail-tail coupling only (Figure 5), and the target CTT-microtubule surface coupling only (Figure 6), show that the thermal cone results solely from the electrostatic repulsion from the negatively charged microtubule surface. Even outside the thermal cone the target CTT has a vanishing effect on the lateral CTT neighbours, and has suprathermal effect upon the immediate CTT neighbours in the same protofilament only when the two CTT

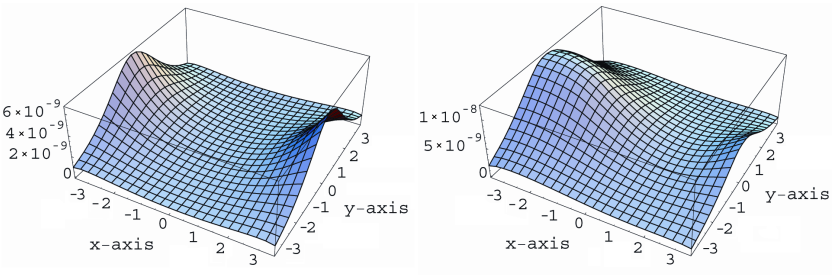

Figure 5: Interaction energy in k_BT units of a target CTT with its CTT neighbours only. (a) All CTTs being perpendicular to the microtubule surface are modeled with $\omega = \frac{2\pi}{3}$ and $\beta_1 = 0$. (b) The same computation with the only difference of CTT_5 being pushed to the edge of its own thermal cone towards the target CTT (in the model this is described as $\theta_5 = \frac{\pi}{5}$ and $\phi_5 = 0$). Depicted is a spatial region with dimensions 3.5×3.5 nm.

neighbours tilt towards each other at distance between the interacting COO^- groups of the order of the Bjerrum length λ_B. From the computations is clear that the only visibly interacting CTT neighbours are those lying in the same protofilament. When the CTT_1 and CTT_5 neighbours are perpendicular to the microtubule surface the interaction energy is 9 orders of magnitude below the thermal energy (Figure 5a), while if one of these neighbours is pushed to the edge of its own thermal cone towards the target CTT the interaction energy is slightly increased up to 8 orders of magnitude below k_BT (Figure 5b). The plots only of the tail-tail coupling show small dependence on the initial CTT orientation, yet the interaction energies are 8 orders of magnitude lower than the interaction with the microtubule surface, hence the total interaction energy surface is not visibly changed. Therefore we conclude that under normal conditions when the CTT neighbours are perpendicular to the microtubule surface (or remain within the volume of their thermal cones) the tail-tail coupling should have no biological significance. A suprathermal tail-tail interaction is possible when an external factor (such as attachment of charged macromolecule) forces two CTTs from the same protofilament to tilt towards each other in direct physical interaction at distance comparable to λ_B. Yet in this case the CTT behaviour will be constrained by the presence of the charged macromolecule itself.

4.2 Mg^{2+} effects on α-CTT dynamics

The α-CTT interaction with positively charged clusters on the microtubule surface such as the Lys394 area on α-tubulin was described by Pal et al. (2001). Results from the same group (Bhattacharya et al., 1994) have shown that Mg^{2+} ions bind with high affinity to tubulin and promote the α-CTT interaction with the Lys394 positive area on the microtubule surface, yet the precise location of Mg^{2+}-binding site remains elusive. The effect specific for Mg^{2+} binding was

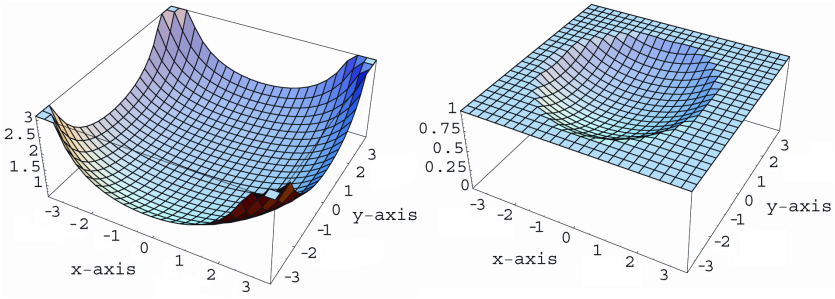

Figure 6: (a) Interaction energy in k_BT units of a target CTT with the microtubule surface only. (b) Visualization of the resulting thermal cone. Depicted is a spatial region with dimensions 3.5×3.5 nm.

not reproduced by addition of Na^+ or Ca^{2+} ions. Mimicking the Mg^{2+} effects can be achieved by the addition of Mn^{2+} ions suggesting that Mn^{2+} ions could also bind, albeit with lesser affinity, to the putative Mg^{2+} binding site on the tubulin surface.

Our results suggest a possible localization of this putative Mg^{2+} binding site. We have shown that the CTT repulsion from the negatively charged microtubule surface predominates and is the sole factor determining the existence of the thermal cone. Since the α-CTT can reach the α-Lys394 area only when in fully stretched conformation (Pal et al., 2001) this implies that the α-CTT must bend over a large area above the tubulin surface and that it is the CTT top that binds the positive microtubule surface spot. However, on its way towards the α-Lys394 area the α-CTT will be repelled back due to the electrostatic repulsion from the negatively charged microtubule surface lying between the α-CTT base and the α-Lys394 area, so the α-CTT will not be capable of binding to the microtubule surface. If however the high affinity Mg^{2+} binding site on tubulin is located between the α-Lys394 area and the α-CTT base, the Mg^{2+} ion will form a positive bridge that will favour the α-CTT-tubulin body interaction. Another possibility that we cannot rule out is the Mg^{2+} (or Mn^{2+}) ion direct bonding with the lowest two COO^- groups of the CTT. This will result in a significant increase of the thermal cone (Figure 7), yet if such an interaction is possible it needs to be experimentally verified.

5 Discussion

In this paper we have developed a model for estimation of the CTTs dynamics and their thermal cones. Since we have conservatively estimated the possible tail-tail coupling and have found it to be 8 orders of magnitude below the thermal energy our results rule out the possibility for generation and propagation of CTT conformational wave as a result of a local CTT perturbation. Even outside the thermal cone the CTT has a subthermal effect on its neigh-

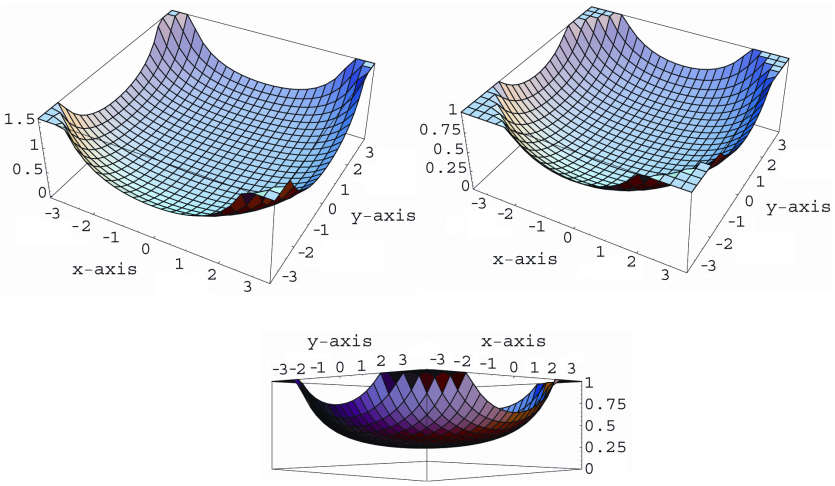

Figure 7: (a) Interaction energy in k_BT units of a target CTT in case of putative Mg^{2+} binding to the CTT lowest two glutamate COO^- groups. (b-c) The thermal cone is visualized by setting the plot range from 0 to 1 k_BT. Depicted is a spatial region with dimensions 3.5×3.5 nm.

bours. Since any local electrostatic CTT perturbation (e.g. CTT interaction with motor protein molecule, or CTT binding to a positive microtubule surface spot) will be screened at a distance of several Debye lengths, we conclude that local electrostatic perturbations cannot propagate along the protofilament of extended CTTs. Also we consider it unlikely that such a local perturbation can be transmitted as ionic waves in the vicinity of MAP molecule to neighboring microtubule 50 nm away since the screening effect will reduce the original electrostatic perturbation over 20 orders of magnitude at that distance.

The computational data we have presented enhance our original model in which the electric currents born by the dendritic or axonal membrane depolarization or hyperpolarization affect simultaneously all CTTs of a given microtubule resulting in a collective CTT motion (Georgiev and Glazebrook, 2006). This is easily explainable since the neuronal electric currents have sufficiently high suprathermal energy not only to order the CTTs within their thermal cones, but also for pushing them out of the thermal cone to interplay with the electrostatic repulsion by the negatively charged microtubule surface. Since the CTTs are modified also by second messenger cascades triggered by G-protein coupled receptors, and CTTs are direct acceptors of paracrinely-secreted molecules such as nitric oxide (NO), we consider the microtubules as integrating all relevant anisotropic signals with the effect resulting from the local electromagnetic field and electric currents acting upon the CTTs (Georgiev et al., 2004).

An interesting issue that needs to be addressed is the fact that *in vivo* CTTs of neuronal microtubules undergo post-translational modifications (PTMs) some of which lead to branching of the tail and/or lead to additional charging of the

tail (Gundersen et al., 1984; Rosenbaum, 2000; Westermann and Weber, 2003). PTMs are responsible for crosstalk between microtubules and intermediate filaments, control of MAP binding, kinesin walk and neuronal differentiation, and as revealed recently by knock out genetic experiments PTMs are vital for proper structural organization of brain (Erck et al., 2005). What might be relevant for the presented here model is to consider the consequences of the polyglutamylation in which a polyglutamate side chain of variable length (up to 20 glutamate residues) is attached, through an isopeptide bond, to the γ-carboxylate group of a glutamate in CTT. One might argue that the extending perpendicularly to the CTT stalk polyglutamate chain might couple two neighbouring CTT along the protofilament. Careful consideration of the reported here model however reveals that this is not the case. In order for the CTT to preserve its mobility the added polyglutamate chain should be relatively short, otherwise the CTT motion will be significantly damped by the cytosol. However even in this case it will be energetically unfavourable for the added polyglutamate chain to be alligned parallely to the microtubule protofilament (x-axis), instead it will be alligned parallely to the y-axis. This is expected due to the cylindrical geometry of the charged microtubule surface and because the distances between the CTTs in neighbouring protofilaments are significantly greater than distances along the protofilament. At best, one might speculate there is a coupling along the 3-start helix under certain special distribution pattern of PTMs, yet at present no study has been undertaken to reveal the *in vivo* nanoscale PTM pattern on the microtubule. Whether PTM coupling between CTTs in adjacent protofilaments is possible *in vivo* and/or what is the biological significance of PTMs via effect on CTT motion remains outside the scope of the current work. An experimentally proved biological function for polyglutamylation is control of kinesin walk and interfering with τ protein attachment, but not that of MAP1B (Larcher et al., 1996; Bonnet et al., 2001).

The essential importance of the current work is that it rules out the significant tail-tail coupling and generation and propagation of CTT conformational waves along the protofilaments as a result of local CTT perturbations. In contrast, it is feasible that the electric currents flowing in the neuronal cytosol during membrane hyper or depolarization have sufficiently high energy to generate collective CTT motion along the protofilament. In this sense the electric currents are "projected" onto the underlying microtubule CTTs and the resultant collective CTT dynamics is determined by the interplay of the electric force exerted on the CTTs by the flowing cytosolic currents and the repulsion of the CTTs from the negatively charged microtubule surface. Therefore we conclude that the current investigation is supportive for a group of models in which the neuronal bioelectric processes interplay with the CTT conformations. This would not be feasible if the local CTT couplings possessed suprathermal energy. Details of our proposed interaction between CTTs and the cytosolic electric field are reviewed in previous publications and novel mathematical models allowing for soliton, or soliton-like solutions of the collective CTT dynamics during neuronal excitations, are currently under investigation.

Appendix: Geometry of COO^- groups under CTT tilting

Here we present the derivations of eqs.(13-15) that seem cumbersome at first glance. Since we have fixed the angle β_1 (actually all β_i) the condition of no axial spinning of the CTT around the main stalk during the tilting, implies that the CTT main stalk from the initial perpendicular position, to the final tilted position moves within the σ-plane in such a fashion that each COO_i^- group remains at the same distance from the σ-plane (see Figure 8), which is equivalent to say that $\angle epq = \angle fhk$. The reader should keep in mind that the imposed condition of no axial spinning during the CTT tilting is not *per se* a restriction on the real CTT dynamics. It is purely mathematical procedure for convertion of the 4-dimensional CTT thermal cone into infinite number of 3-dimensional CTT thermal cones that can be printed out and serve for illustration of the discussion. *In vivo* the CTT might undergo axial spinning (β_1 is a variable) and if one needs to compute the interaction energy between the CTT and its environment he/she must know not only θ and ϕ, but also β_1.

Further we project the location of the COO_i^- group onto the xy- and σ-planes via orthogonal projection. On Figure 8 we have depicted the projections of the COO_1^- group but the geometry and the equations written in general form with index are valid for arbitrary COO_i^- group. We have the following parallelograms: $eqba$, $oaep$, $opqb$, $fkcd$, $abcd$, $absu$, $uscd$ and $orhs$. One also finds $\angle kmd = \theta$ because $\overrightarrow{om} \perp \overrightarrow{oz}$ and $\overrightarrow{oh} \perp \overrightarrow{hm}$.

The following list of trigonometric equations holds: $\overline{pe} = \overline{hf} = \overline{oa} = R$; $\overline{oh} = \overline{op} = L_i$; $\overline{eq} = \overline{fk} = \overline{ab} = \overline{cd} = \overline{us} = R\sin(\phi - \beta_i)$; $\overline{pq} = \overline{ob} = \overline{hk} = R\cos(\phi - \beta_i)$; $\overline{sd} = \overline{hk}\cos\theta$; $\overline{or} = L_i\cos\theta$; $\overline{rh} = \overline{os} = L_i\sin\theta$; $\overline{od} = \overline{sd} + \overline{os}$; $\overline{ac} = \overline{bd} = \overline{od} - \overline{ob}$.

For the x-coordinate of the COO_i^- we have the projection of $\overline{oa} = R$ onto the x-axis (here is where the $\cos\beta_i$ appears) plus the projection of $\overline{ac}$ onto the x-axis (here is where the $\cos\phi$ appears), and we get eq.13. Similarly one projects onto the y-axis with the sine of the corresponding angles getting eq.14. What remains is to estimate the z-coordinate. For z we have $\overline{or}$ minus the projection of $\overline{hk}$ onto the z-axis (here is where $\sin\theta$ appears) and we get eq.15.

References

[1] Baker NA, Sept D, Joseph S, Holst MJ, McCammon JA. (2001) Electrostatics of nanosystems: application to microtubules and the ribosome. *Proc. Natl. Acad. Sci. USA* **98**: 10037-10041.

[2] Bhattacharyya B, Sackett DL, Wolff J. (1985) Tubulin, hybrid dimers, and tubulin S. Stepwise charge reduction and polymerization. *J. Biol. Chem.* **260**: 10208-10216.

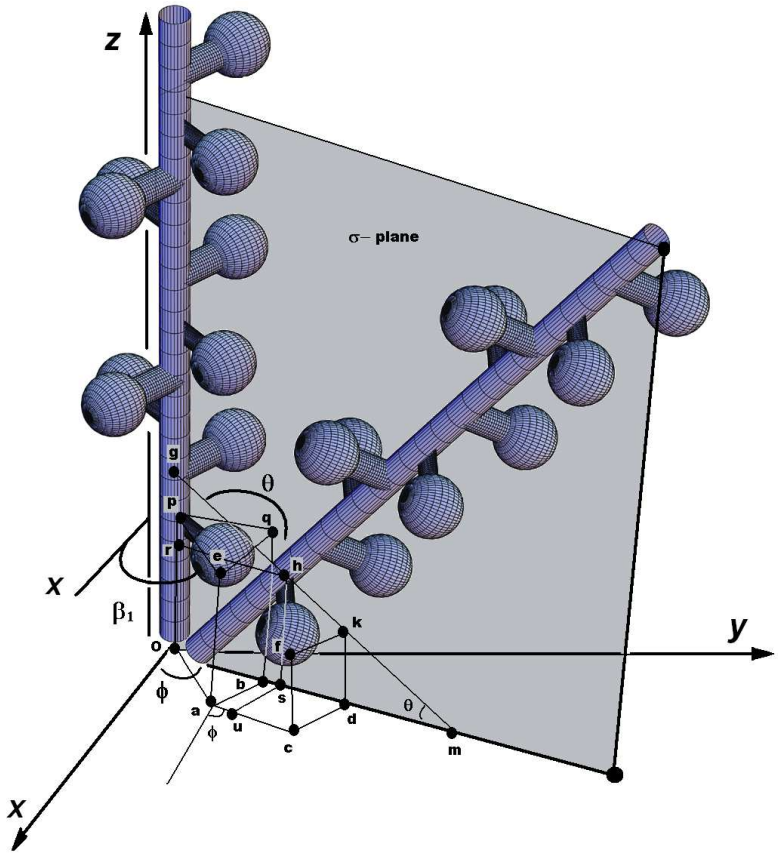

Figure 8: Geometry of COO_i^- groups under CTT tilting.

[3] Bhattacharya A, Bhattacharyya B, Roy S. (1994) Magnesium-induced structural changes in tubulin. *J. Biol. Chem.* **269**: 28655-28661.

[4] Bonnet C, Boucher D, Lazereg S, Pedrotti B, Islam K, Denoulet P, Larcher JC. (2001) Differential binding regulation of microtubule-associated proteins MAP1A, MAP1B, and MAP2 by tubulin polyglutamylation. *J. Biol. Chem.* **276**: 12839-12848.

[5] Brocard JB, Rajdev S, Reynolds IJ. (1993) Glutamate-induced increases in intracellular free Mg^{2+} in cultured cortical neurons. *Neuron* **11**: 751-757.

[6] Cherstvy AG, Winkler RG. (2004) Complexation of semiflexible chains with oppositely charged cylinder. *J. Chem. Phys.* **120**: 9394-9400.

[7] Chitanvis SM. (2003) Theory of polyelectrolytes in solvents. *Phys. Rev. E* **68**: 061802.

[8] Debye P, Hückel E. 1923. Zur theorie der elektrolyte. I. Gefrierpunktserniedrigung und verwandte erscheinungen. *Physikalische Zeitschrift* **24**: 185-206.

[9] de Pablo PJ, Schaap IAT, Schmidt CF. (2003) Observation of microtubules with scanning force microscopy in liquid. *Nanotechnology* **14**: 143-146.

[10] Diaz JF, Valpuesta JM, Chacon P, Diakun G, Andreu JM. (1998) Changes in microtubule protofilament number induced by taxol binding to an easily accessible site. *J. Biol. Chem.* **273**: 33803-33810.

[11] Erickson HP, Stöffler D. (1996) Protofilaments and rings, two conformations of the tubulin family conserved from bacterial FtsZ to α/β and γ-tubulin. *J. Cell Biol.* **135**: 5-8.

[12] Erck C, Peris L, Andrieux A, Meissirel C, Gruber AD, Vernet M, Schweitzer A, Saoudi Y, Pointu H, Bosc C, Salin PA, Job D, Wehland J. (2005) A vital role of tubulin-tyrosine-ligase for neuronal organization. *Proc. Natl. Acad. Sci. USA* **102**: 7853-7858.

[13] Fogolari F, Zuccato P, Esposito G, Viglino P. (1999) Biomolecular electrostatics with the linearized Poisson-Boltzmann equation. *Biophys. J.* **76**: 1-16.

[14] Georgiev DD. (2003) Electric and magnetic fields inside neurons and their impact upon the cytoskeletal microtubules. `http://cogprints.org/3190/`

[15] Georgiev DD. (2004) Solitonic effects of the local electromagnetic field on neuronal microtubules - tubulin tail sine-Gordon solitons could control MAP attachment sites and microtubule motor protein function. `http://cogprints.org/3894/`

[16] Georgiev DD, Glazebrook JF. (2006) Dissipationless waves for information transfer in neurobiology - some implications. *Informatica* **30**: 221-232.

[17] Georgiev DD, Glazebrook JF. (2007) Subneuronal processing of information by solitary waves and stochastic processes. In: *Nano and Molecular Electronics Handbook*, Lyshevski S. (ed.), CRC Press, Francis & Taylor, USA.

[18] Georgiev DD, Papaioanou SN, Glazebrook JF. (2004) Neuronic system inside neurons: molecular biology and biophysics of neuronal microtubules. *Biomed. Rev.* **15**: 67-75.

[19] Gundersen GG, Kalnoski MH, Bulinski JC. (1984) Distinct populations of microtubules: tyrosinated and nontyrosinated α-tubulin are distributed differently in vivo. *Cell* **38**: 779-789.

[20] Hansen JP, Löwen H. (2000) Effective interactions between electric double layers. *Ann. Rev. Phys. Chem.* **51**: 209-242.

[21] Hille B. (2001) *Ion Channels of Excitable Membranes*. Sinauer Associates, Sunderland, Massachusetts.

[22] Hirokawa N. (1998) Kinesin and dynein superfamily proteins and the mechanism of organelle transport. *Science* **279**: 519-526.

[23] Hyman AA, Chretien D, Arnal I, Wade RH. (1995) Structural changes accompanying GTP hydrolysis in microtubules: information from a slowly hydrolyzable analogue guanylyl-(α,β)-methylene-diphosphonate. *J. Cell Biol.* **128**: 117-125.

[24] Jimenez MA, Evangelio JA, Aranda C, Lopez-Brauet A, Andreu D, Rico M, Lagos R, Andreu JM, Monasterio O. (1999) Helicity of α(404-451) and β(394-445) tubulin C-terminal recombinant peptides. *Protein Sci.* **8**: 788-799.

[25] Larcher JC, Boucher D, Lazereg S, Gros F, Denoulet P. (1996) Interaction of kinesin motor domains with α- and β-tubulin subunits at a τ-independent binding site. Regulation by polyglutamylation. *J. Biol. Chem.* **271**: 22117-22124.

[26] Lloyd PG, Hardin CD. (1999) Role of microtubules in the regulation of metabolism in isolated cerebral microvessels. *Am. J. Physiol. Cell Physiol.* **277**: C1250-C1262.

[27] Nogales E, Wolf SG, Downing KH. (1998) Structure of the α/β tubulin dimer by electron crystallography. *Nature* **391**: 199-203.

[28] Nogales E. (2000) Structural insights into microtubule function. *Ann. Rev. Biochem.* **69**: 277-302.

[29] O'Shaughnessy B, Yang Q. (2005) Manning-Oosawa counterion condensation. *Phys. Rev. Lett.* **94**: 048302.

[30] Pal D, Mahapatra P, Manna T, Chakrabarti P, Bhattacharyya B, Banerjee A, Basu G, Roy S. (2001) Conformational properties of α-tubulin tail peptide: implications for tail-body interaction. *Biochemistry* **40**: 15512-15519.

[31] Pauling L, Corey RB, Branson HR. (1951) The structure of proteins: two hydrogen-bonded helical configurations of the polypeptide chain. *Proc. Natl. Acad. Sci. USA* **37**: 205-211.

[32] Poon WCK, Andelman D. (2006) *Soft Condensed Matter Physics in Molecular and Cell Biology*. Scottish Graduate Series Vol. 59. Taylor & Francis, CRC Press.

[33] Purich DL. (2001) Enzyme catalysis: a new definition accounting for noncovalent substrate- and product-like states. *Trends Biochem. Sci.* **26**: 417-421.

[34] Rosenbaum J. (2000) Cytoskeleton: Functions for tubulin modifications at last. *Curr. Biol.* **10**: R801-R803.

[35] Sackett DL, Wolff J. (1986) Proteolysis of tubulin and the substructure of the tubulin dimer. *J. Biol. Chem.* **261**: 9070-9076.

[36] Skiniotis G, Cochran JC, Mueller J, Mandelkow E, Gilbert SP, Hoenger A. (2004) Modulation of kinesin binding by the C-termini of tubulin. *EMBO J.* **23**: 989-999.

[37] Sontag E, Nunbhakdi-Craig V, Lee G, Brandt R, Kamibayashi C, Kuret J, White CL, Mumby MC, Bloom GS. (1999) Molecular interactions among protein phosphatase 2A, τ, and microtubules. Implications for the regulation of τ phosphorylation and the development of tauopathies. *J. Biol. Chem.* **274**: 25490-25498.

[38] Stankovich J, Carnie SL. (1996) Electrical double layer interaction between dissimilar spherical colloidal particles and between a sphere and a plate: nonlinear Poisson-Boltzmann theory. *Langmuir* **12**: 1453-1461.

[39] Uversky VN. (2002a) Natively unfolded proteins: a point where biology waits for physics. *Protein Sci.* **11**: 739-756.

[40] Uversky VN. (2002b) What does it mean to be natively unfolded? *Eur. J. Biochem.* **269**: 2-12.

[41] Uversky VN. (2002c) Cracking the folding code: Why do some proteins adopt partially folded conformation, whereas other don't? *FEBS Lett.* **514**: 181-183.

[42] Vale RD, Banker G, Hall ZW. (1992) The neuronal cytoskeleton. In: Hall, Z.W. (Ed.), *An Introduction to Molecular Neurobiology*. Sinauer Associates, Sunderland, MA, pp. 247-280.

[43] Westermann S, Weber K. (2003) Post-translational modifications regulate microtubule function. *Nat. Rev. Mol. Cell Biol.* **4**: 938-947.

[44] Zeng WZ, Liu TP. (1993) Effects of tetrandrine on free intracellular Ca^{2+} in isolated rat brain cells. *Acta Pharmacol. Sin.* **14**: 397-400.